DOI: 10.1021/ma902494v

Macromolecules
ARTICLE

Remediation of Line Edge Roughness in Chemical Nanopatterns by the Directed Assembly of Overlying Block Copolymer Films

Mark P. Stoykovich*

Department of Chemical and Biological Engineering, University of Colorado—Boulder, Boulder, Colorado 80309

Kostas Ch. Daoulas and Marcus Müller

Institut für Theoretische Physik, Georg-August Universität, 37077 Göttingen, Germany

Huiman Kang, Juan J. de Pablo, and Paul F. Nealey

Department of Chemical and Biological Engineering, University of Wisconsin—Madison, Madison, Wisconsin 53706

Received November 11, 2009; Revised Manuscript Received January 18, 2010

ABSTRACT: Block copolymer structures have been directed to assemble on chemically patterned surfaces with the domain interfaces oriented perpendicular to the substrate. Such methods have been pursued for lithographic applications to achieve long-range order in the assembled structures and, potentially more important, provide nanometer-level control over the interfaces between structures. The chemically striped surfaces used for the directed assembly of lamellae are patterned by top-down lithographic techniques and thus often have rough edges between the regions of different chemistry. Here we quantitatively characterize, using experiments and molecular-level simulations, the propagation of line edge roughness from the chemically patterned surfaces into the interfaces between domains of block copolymer lamellae as a function of the wavelength, amplitude, and geometry of the roughness. Two geometries of surface pattern roughness are considered with oscillatory neighboring interfaces that are either in-phase or out-of-phase. Block copolymer lamellae of poly(styrene-*block*-methyl methacrylate) effectively self-corrected surface patterns with small wavelength in-phase and out-of-phase roughness such that little or no memory of the substrate pattern roughness could be observed at the top surface of a 40 nm thin film. Larger wavelength in-phase roughness, and to a lesser extent larger wavelength out-of-phase roughness, propagated farther from the surface pattern such that the domain interfaces between block copolymer lamellae maintained the roughness throughout the film. These self-healing capabilities of block copolymers will be essential for lithographic applications with tight tolerances on line edge roughness and line width control, *e.g.*, in patterning transistor gates.

Introduction

Advanced lithographic techniques and photoresist materials are rapidly approaching their useful limits in patterning at the ever-decreasing dimensions required for semiconductor devices such as transistors in integrated circuits (*e.g.*, in microprocessor units (MPU)) and dynamic random access memory (DRAM). The semiconductor industry has specified the requirements for photoresists and lithographic exposure tools at future technology nodes in the International Technology Roadmap for Semiconductors (ITRS).[1] Particularly troublesome has been the inability of conventional photoresist materials to meet the critical dimension control (CD referring to the dimension of the smallest patterned feature of importance, *e.g.*, the transistor gate length in MPUs) and line edge roughness (LER) requirements, both of which should have been at sub 3 nm levels by the year 2009.[1,2] The frequency of the line edge roughness, in addition to the magnitude of the LER, is an important consideration for the devices to be fabricated and affects the operation of transistors,[3−6] interconnect wire resistances,[7,8] and dopant concentration profiles. For example, small wavelength roughness influences the operation of individual transistors (local variations in gate length affect the threshold voltage and current leakage, and thus overall power consumption), while large wavelength roughness affects the operation of transistor groups (variations in transistor speeds can cause integrated circuit timing issues).[4,9,10]

Self-assembly approaches using block copolymers are actively being pursued as a next generation lithography technique, not only due to the ability of such materials to spontaneously form large arrays of linear or cylindrical structures at the necessary resolution, but also because of the molecular-level control such materials provide over the structure dimensions and interfaces.[11−15] In the case of block copolymer lithography with symmetric copolymers, line and space structures can be fabricated with line edges defined by the interfaces between lamellar domains. The width and structure of the interfaces, influenced in part by thermally excited capillary waves, are governed by system parameters such as the Flory−Huggins interaction parameter and the invariant degree of polymerization.[16,17] Assembly of lamellar structures into arrays with long-range order is complicated by low free-energy defects such as disclinations,

*To whom correspondence should be addressed. E-mail: mark.stoykovich@colorado.edu.

 Published on Web 02/10/2010

dislocations, and bending of the domain interfaces with relatively large radii of curvatures compared to the domain periodicity. Directed assembly of block copolymers on chemical surface patterns[18−31] is an attractive technique for self-assembling structures with long-range order and a high degree of perfection, that are positioned with respect to the substrate, and in geometries relevant to the patterning of semiconductor devices.[22,23] Preferential wetting of the block copolymer domains on the surface patterns in this approach greatly enhances the energetic penalty of standard block copolymer defects and therefore prohibits their formation. In addition, block copolymers in thin films have a demonstrated ability to correct for small defects in the surface pattern[24,32] and provide a degree of CD control over the assembled structures.[33]

The ability of block copolymers to self-heal roughness in the chemical surface pattern has not been demonstrated experimentally, although a recent investigation using phenomenological approaches and molecular-level simulations provides insight into such a behavior.[32] Chemical surface patterns with model in-phase (undulation roughness) or out-of-phase (peristaltic roughness) geometries, as specified by neighboring edges that were sinusoidal with a specific wavelength, were predicted to induce roughness in the lamellar interfaces. The propagation of the roughness from the chemical surface pattern into the interfaces of the block copolymer lamellae was found to be dependent on the roughness geometry, roughness wavelength, and film thickness. One conclusion, for example, was that the roughness in the block copolymer interface decays more rapidly in thick films than in thin films. The simulations also predicted the conditions of the substrate and block copolymer for which the roughness in the surface pattern would propagate in the block copolymer interfaces through the entire thin film and be observed at the top, free surface of the film.

Here we present an experimental characterization of the line edge roughness in block copolymer lamellae that propagates from the substrate chemical pattern to the top-surface of the polymer film. Direct comparisons are made to predictions from Single-Chain-in-Mean-Field simulations. A spectral analysis of the self-assembled lamellar structures using critical dimension scanning electron microscopy (CD−SEM) provides information on the average shape of the polymer−polymer domain interfaces. The average interfaces between block copolymer domains are compared to the roughness present in the chemical surface patterns on which the block copolymers were directed to assemble. Model surface patterns were fabricated with oscillatory boundaries between the stripes, thus the response of the block copolymer interfaces to particular frequencies of roughness in the surface pattern could be monitored. The neighboring boundaries had either undulation or peristaltic roughness (see Figure 1a) with a predominant wavelength equal to or twice the lamellar period of the block copolymer. Block copolymer domains directed to assemble on these surface patterns with supplemental roughness were found to self-heal the roughness in the surface pattern to varying degrees dependent upon the geometry and wavelength of the roughness and the distance from the substrate. The experimental observations for this remediation of roughness present in the chemical surface pattern are in good agreement with the corresponding theoretical predictions.

Methods and Materials

Directed Assembly on Chemical Surface Patterns with Controlled LER. A generalized scheme for the directed assembly of block copolymers on chemical surface patterns is shown in Figure 1b. In the first step, chemical surface patterns were fabricated in a polystyrene (PS, 9.5 kg mol^{-1}) brush imaging layer covalently grafted on silicon substrates such that the

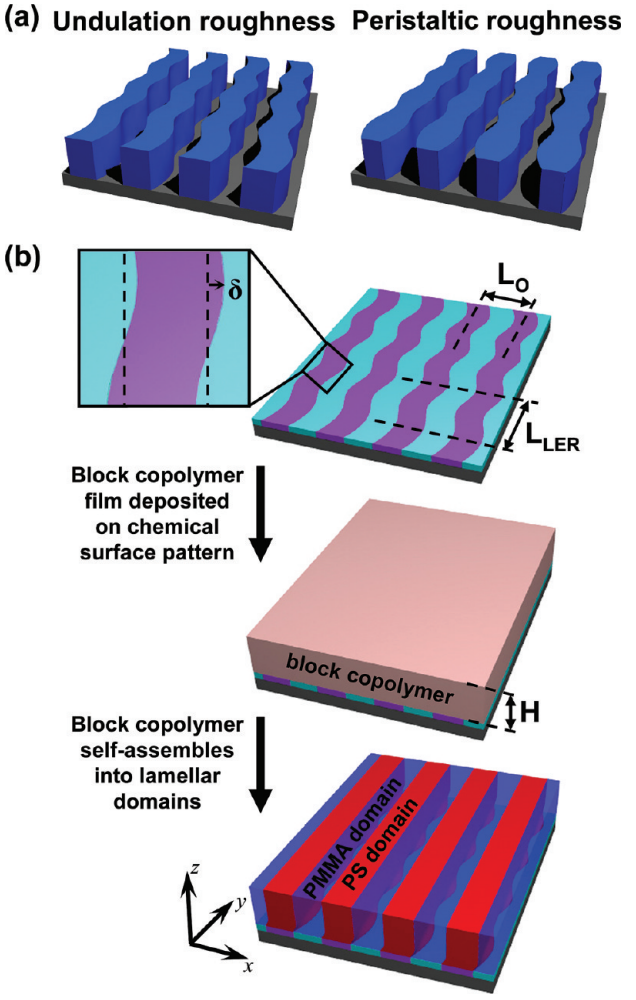

Figure 1. Schematics of (a) undulation and peristaltic roughness in a periodic array of lines and (b) the directed assembly of block copolymers on chemical surface patterns with edge roughness. In part b, the top frame shows a chemical surface pattern having undulation roughness between the PMMA and PS preferential regions in light blue and purple, respectively. The periodicity of the chemically preferential stripes is L_O equal to the bulk lamellar spacing and the periodicity of the roughness along the edge of each stripe is L_{LER}. A block copolymer film of thickness H is deposited and annealed such that PMMA (blue) and PS (red) lamellae are directed to assemble in registry with the surface pattern.

alternating stripes had distinct chemistries and surface energies. The fabrication process used electron beam lithography to define the surface pattern in a photoresist film that subsequently acted as a mask for an oxygen plasma treatment that chemically modified the PS brush (details for this procedure can be found in refs 22 and 34). The periodicity of the chemical surface pattern (L_S) was chosen to closely match the periodicity of the block copolymer lamellae (L_o), such that in this case L_S = 70 nm. The geometry of the chemically patterned stripes, specifically the line edges between the different chemical regions, was controlled during fabrication such that undulation (in-phase line edges) or peristaltic (out-of-phase line edges) roughness was programmed into the surface pattern. The periodicity and amplitude of this supplemental roughness was L_{LER} and δ_o, respectively. The approximately sinusoidal boundaries were superimposed with other frequencies of low amplitude roughness inherent to the photoresist and exposure tool used for patterning.

Lamellar-forming block copolymer films of thickness $H \approx 40$ nm were deposited on the patterned surfaces and annealed at an elevated temperature below the order−disorder

transition temperature (190 °C for 3 days). The microphase separated lamellar domains that assembled preferentially wet the different stripes of the surface pattern and were oriented perpendicular to the substrate. In addition, the lamellae were ordered without dislocation and disclination defects over greater than 2 μm by 2 μm areas, and were spatially registered with the underlying surface pattern. A symmetric ternary blend of 60 wt % poly(styrene-block-methyl methacrylate) (PS-*b*-PMMA, 104 kg mol^{-1} total, 48 wt % PS), 20 wt % PS homopolymer (45 kg mol^{-1}), and 20 wt % poly(methyl methacrylate) homopolymer (PMMA, 46.5 kg mol^{-1})) was used here, but this copolymer system behaves similarly to a pure symmetric diblock copolymer in thin films and on chemical surface patterns.[35] The polymers were used as received from Polymer Source, Inc. (Dorval, Canada). Figure 1(b) illustrates a case in which (1) the block copolymer lamellae at the substrate perfectly follow the undulation roughness in the surface pattern and (2) the interfaces between lamellar domains at the top surface of the film have been self-corrected to straight lines, *i.e.*, zero line edge roughness. This morphology is similar to what has been predicted using the simulations on these types of substrate patterns.[32]

The structures of the block copolymer lamellae at the free surface and the chemically patterned surface were characterized using top-down imaging techniques. The lamellar structure at the chemically pattern surface was determined after the directed assembly process by flipping over the film for imaging purposes. In this case, chemical surface patterns were defined in PS polymer brushes on 100 nm SiO_2 sacrificial films deposited on Si wafers by chemical vapor deposition. Directed assembly of the block copolymer using these chemically patterned surfaces resulted in lamellar structures identical on the top surface of the film to those assembled on Si substrates. Subsequent treatment by ~1 vol % HF etched away the SiO_2 layer, and thereby allowed the block copolymer films to float in a water bath and be flipped over onto a second Si support for imaging.

Characterization of Line Edge Roughness in Lamellar Interfaces. Top-down scanning electron micrographs (LEO 1550-VP) were captured at a magnification of 100 000 ($d \approx 1.1$ nm/pixel is the sampling interval) and analyzed to characterize the line edge roughness of the block copolymer lamellae and the chemical surface pattern. Line edges were extracted from the grayscale images by implementing an edge detection algorithm that first applied Gaussian smoothing along each row of pixels (x direction) perpendicular to the line edge (y direction) to eliminate noise. Then a single threshold point (typically 40−50% of the grayscale) was used to determine the interface position. The deviation in the x direction of the interface position from a linear best fit, $\delta_i(y)$, was then calculated for each line edge i in the SEM image. Undoubtedly the shapes and dimensions of the line edges were influenced by the characterization technique (*e.g.*, swelling of the PS domains), the quality of the images (*e.g.*, resolution and contrast between domains), the image postprocessing procedure, and the edge detection algorithm. Consistent imaging and characterization procedures were maintained throughout and facilitated a quantitative comparison between the line edges in the surface pattern and block copolymer structures.

The power spectra density (PSD) is plotted as a function of spatial frequency ($q = 2\pi/r$ where r is a distance along the line edge) and was calculated as the discrete Fourier transform of the normalized autocorrelation function along the line edge averaged over many consecutive line edges. The PSD is thus calculated by

$$PSD(q) = \sum_{m=0}^{P-1} \bar{R}(md) e^{iqmd} = \sum_{m=0}^{P-1} \bar{R}(md) e^{2\pi ikm/P}$$

where the spatial frequency q is defined as

$$q = \frac{2\pi k}{d \cdot P}, \quad k = -\frac{P}{2}, \ldots, \frac{P}{2}$$

The normalized autocorrelation function averaged over $n \geq 25$ consecutive line edges is

$$\bar{R}(md) = \frac{1}{n} \sum_{i=1}^{n} R_i(md)$$

and the normalized autocorrelation function along an individual line edge labeled i is

$$R_i(md) = 1 - \left[\left(\frac{1}{P-m} \sum_{j=1}^{P-m} (\delta_i(j+m) - \delta_i(j))^2 \right) / 2\sigma_i^2 \right]$$

Other parameters are defined as follows: P is the number of consecutive pixels along each line edge that were analyzed in the image ($P \geq 520$); m is an integral number of pixels along the line edge $m = 0,\ldots,P-1$; d is the distance between neighboring pixels or sampling interval; and σ_i is the root mean squared deviation of line edge i from its linear fit; *i.e.*[3]

$$\sigma_i = \sqrt{\sum_{j=1}^{P} \delta_i{}^2(j)/P}$$

Sinusoidal fits of the average interface deformations were performed for the block copolymer lamellae and the corresponding chemical surface patterns. Line edges were spatially averaged assuming (1) a 0° or 180° phase shift in roughness between neighboring line edges

$$\bar{\delta}'(y) = \frac{1}{n} \sum_{i=1}^{n} \delta_i(y)$$

depending on whether the roughness has a undulation or peristaltic geometry, respectively, and (2) a L_{LER} periodicity of roughness in the line edge

$$\bar{\delta}(y) = \frac{1}{2l+1} \sum_{j=-l}^{l} \bar{\delta}'(y + jL_{LER})$$

where $2l+1$ is the integral number of full L_{LER} periods along the length of each line edge). This average was again calculated over $n \geq 25$ consecutive line edges. The averaged line edge $\bar{\delta}(y)$ was subsequently fit using a least-squares algorithm to a sinusoidal curve of the form $h(y) = f \sin(2\pi y/L_{LER})$ for the block copolymer lamellae or $h(y) = \delta_o \sin(2\pi y/L_{LER})$ for the chemical surface pattern, where the roughness amplitude is given by f or δ_o. The amplitude of roughness in the interfaces of the block copolymer lamellae at the free surface $f(z = 40$ nm) is reported relative to the corresponding surface pattern roughness δ_o.

Modeling Approach. Molecular-level simulations can provide significant insight into the assembly of block copolymer morphologies and can characterize the copolymer nanostructures in three-dimensions at length scales and levels of details difficult to examine experimentally.[32,36,37] The Single-Chain-in-Mean-Field (SCMF) simulation technique has been shown to be an efficient modeling approach for studying structure formation in assembling polymeric systems on a mesoscopic level. This approximate particle-based method retains the efficiency of self consistent field approaches, by which it was originally inspired, providing at the same time an accurate description of the

fluctuations. It has been elaborated in detail elsewhere,[38,39] therefore only a brief outline is presented here.

The polymer connectivity is described within a bead−spring model. Here the PS-*b*-PMMA diblock chains are discretized into $N = 15 + 17$ effective segments, while the PS and PMMA homopolymers contain $N_{PS} = 12$ and $N_{PMMA} = 13$ monomers, respectively. The polymer chain number density n/V matches the experimental system, with an invariant degree of polymerization of $\tilde{N} = (nR_e^3/V)^2 = 16384$, where R_e is the end-to-end distance of the unperturbed diblock chain (see discussion below) and we use the same blend composition as the experimental systems. The nonbonded interactions are described via a coarse-grained density functional, $F[\{\varphi_\alpha(\mathbf{r})\}]$, of the local volume fractions, $\varphi_\alpha(\mathbf{r})$, of the bead species α, which is either styrene and methyl methacrylate. The interactions of an α-species bead with its surroundings can be described introducing the external fields $W_\alpha(\mathbf{r}) = \delta F/\delta\varphi_\alpha$. These fields are frequently recalculated using the spatial distribution of the components obtained by mapping the coordinates of all the beads in a given configuration onto a cubic lattice. The grid size selected for calculating the densities sets the interaction range and the lowest resolvable length scale. Between updates, the fields are considered as stationary and the chains evolve in them via a short Monte Carlo (MC) simulation. The frequent recalculation of the fields recovers the correlations between the molecules and, in the limit that the external fields follow the system configurations instantaneously, SCMF simulations become accurate.[39] A short decoupling of interactions ("quasi-instantaneous field approximation") does not compromise the accuracy of the method and allows for an efficient implementation on parallel computers.

The functional $F[\{\varphi_\alpha(\mathbf{r})\}]$ is selected according to the specifics of the system to be studied.[40] The form used here has been frequently employed[41] in self consistent field studies of copolymer systems and accounts for the incompatibility of styrene and methyl methacrylate monomers through a Flory−Huggins interaction with strength, $\chi N = 37.6$. The limited compressibility of the polymeric liquid is captured via Helfand's quadratic functional.[42] The polymer beads interact with the chemical pattern through a potential that is short ranged in the z direction normal to the substrate and has the form: $U(x,y,z) = \Lambda N g(x,y) \exp[-z^2/2\varepsilon^2]$. The value $\varepsilon = 0.15\ R_e$ controls the interaction range while the lateral structure of the pattern is encoded in $g(x,y)$, which takes the values 1 or −0.6 depending on whether the (x,y) point on the substrate prefers styrene or methyl methacrylate. The magnitude of the interaction strength is given by $\Lambda N = 3$ and can be only approximated for the experimental system due to the complex procedure used to chemically pattern the substrate. The polymer−air interface at the free surface of the films is modeled as a neutral hard wall. The characteristic length scale of the simulations, R_e, can be related to the experimental systems by comparing the corresponding bulk lamellar spacings $L_o = 2.26R_e$ and $L_o = 70$ nm, respectively.

The surface patterns used in the simulations are an idealized analogue of the chemical surface patterns manufactured experimentally. They consist of stripes with a period, L_S, equal to the period of the bulk lamellae (*i.e.*, $L_S = L_o = 70$ nm) and with periodically modulated edges. This modulation takes the form

$$\delta_o \sin\left(\frac{2\pi}{L_{LER}} y + \varphi\right)$$

where $\delta_o = 6.16$ nm is the pattern LER amplitude and y is the coordinate along the stripe edge.[32] The characteristic roughness wavelength, L_{LER}, was selected to match the cases of $L_{LER} = 70$ nm and $L_{LER} = 140$ nm considered in the experiments, while the proper choice of the phase shift factor, φ, creates patterns with peristaltic and undulation roughness. The chemical surface patterns considered in the SCMF simulations of the current work are shown in Figure 7, parts a (undulation pattern LER) and b (peristaltic pattern LER) enclosed in red and black boxes for the two roughness wavelengths L_{LER}. The purple regions are preferentially wet by the PS component of the block copolymer, while the light blue regions are preferentially wet by the PMMA component. Finally, the film thickness in the model systems was chosen to be similar to the experiments with $H = 44.04$ nm.

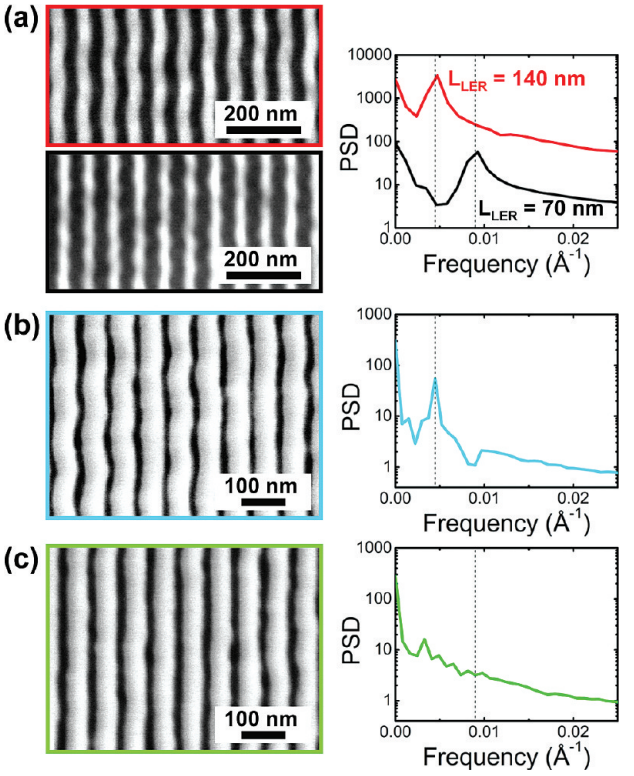

Figure 2. Characterization of PS-*b*-PMMA lamellae directed to assemble on chemical surface patterns with undulation roughness. (a) Top-down SEM images and PSD analyses of the line edge roughness for photoresist patterned with undulation roughness having $L_{LER} = 140$ nm (red, top frame) and 70 nm (black, bottom frame). (b) SEM image and PSD of block copolymer lamellae assembled on surface patterns with $L_{LER} = 140$ nm undulation roughness. (c) SEM image and PSD of block copolymer lamellae assembled on surface patterns with $L_{LER} = 70$ nm undulation roughness. The dashed vertical lines in the PSD plots indicate the frequencies corresponding to $L_{LER} = 140$ and 70 nm.

Results and Discussion

The average shape of block copolymer lamellae directed to assemble on chemical surface patterns with undulation roughness of wavelength $L_{LER} = L_S$ or $2L_S$ (70 or 140 nm) is characterized in Figures 2 and 3. Figure 2a shows the patterned photoresist used to generate the chemical surface pattern and the power spectral density of the extracted line edges. Chemical surface patterns with undulation roughness having the periodicities L_{LER} were readily fabricated as demonstrated by the first-order peaks in the PSD spectra of Figure 2a. Throughout this work the chemical surface pattern has been assumed to be identical to that of the patterned photoresist mask because of the complexity in imaging and characterizing chemically heterogeneous brush surfaces at these length scales. Roughness in the surface patterns at much different wavelengths than L_{LER} arises from the electron beam lithography process used to fabricate the chemically modified surfaces and is manifested as background in the frequency spectrum in the PSDs. This additional roughness, however, does not obscure the predominant roughness with wavelength L_{LER}.

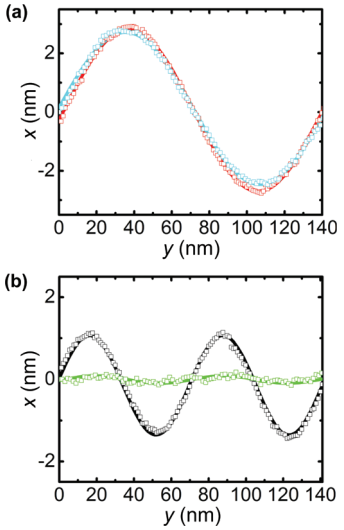

Figure 3. Average deformation $\bar{\delta}(y)$ of the experimental block copolymer interfaces and chemical surface patterns as a function of position along the interfaces (in the y-direction) for undulation surface pattern roughness with (a) L_{LER} = 140 nm and (b) L_{LER} = 70 nm. The experimental data and sinusoidal fits are shown as open circles and continuous curves of the same color, respectively. Red and black colors indicate the average shape of the chemical surface pattern, while blue and green colors indicate the lamellar interfaces at the top of the block copolymer film directed to assemble on such surfaces. The lamellar interfaces are assumed to be in-phase with the corresponding chemical surface pattern.

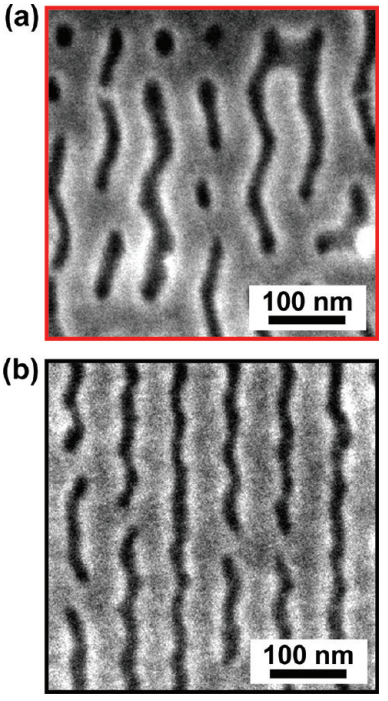

Figure 4. SEM images of the bottom surface of the block copolymer films assembled on chemical surface patterns with undulation roughness of periodicity (a) L_{LER} = 140 nm and (b) L_{LER} = 70 nm.

Parts b and c of Figure 2 show the top surface of block copolymer lamellae directed to assemble on chemical surface patterns with undulation roughness of wavelength L_{LER} = 140 and 70 nm, respectively. Block copolymers self-heal undulation roughness in the chemical surface patterns, but the degree to which the surface pattern roughness propagates in the thin films is a function of the roughness periodicity, L_{LER}. Lamellae assembled on the L_{LER} = 140 nm surfaces displayed undulation roughness on the top surface of the 40 nm thick films as detected by a discernible peak at 140 nm in the PSD spectra in Figure 2b. Undulation surface pattern roughness with L_{LER} = 70 nm, on the other hand, did not propagate in the interface between domains of the block copolymer through this film thickness to the surface of the film. There are no discernible peaks at 70 nm in the PSD spectra in Figure 2c indicating that the average interface between copolymer domains was not dominated by roughness at this particular wavelength. Similar top-down SEM images and power spectra have been observed for the interfaces between domains (or line edges) of block copolymer lamellae assembled on surface patterns without supplemental roughness.

The average interface position of the block copolymer lamellae and the corresponding average chemical surface patterns are characterized in Figure 3 for undulation roughness with L_{LER} = 140 and 70 nm. The experimental top-down SEM images, portions of which are shown in Figure 2, were used to determine the spatially averaged interface deformation $\bar{\delta}(y)$ as a function of y-position along the line edge (shown as data points in Figure 3). Periodic curves with the general sinusoidal form $h(y,z) = f(z)\sin(2\pi y/L_{LER})$ closely fit the average interface positions and are shown as solid lines. The amplitude of the average interface deformation, $f(z)$, depends on the distance z from the chemically patterned substrate. Figure 3a characterizes the L_{LER} = 140 nm undulation roughness case and indicates that the interface deformation in the block copolymer lamellae at the top of the 40 nm film has a similar amplitude ($f(z = 40\text{ nm})$ = 2.6 nm) to the chemical surface pattern (δ_o = 2.9 nm). The relative amplitude of roughness is therefore $f(z = 40\text{ nm})/\delta_o$ = 0.91 and indicates strong propagation of the L_{LER} = 140 nm undulation roughness throughout the block copolymer film. In stark contrast, the average interface deformation for the L_{LER} = 70 nm undulation roughness as shown in Figure 3b is greatly diminished in the block copolymer lamellae compared to the chemical surface pattern with $f(z = 40\text{ nm})/\delta_o$ = 0.073. This real-space characterization of the average interface positions supports the PSD results in Figure 2 and indicates that the block copolymer lamellae can correct for undulation roughness in the surface pattern to varying degrees dependent on the L_{LER} periodicity of the roughness. Note that the phase of the lamellar interface at the top of the film relative to the chemical surface pattern has not been determined and is assumed to be in-phase for the purposes of plotting $\bar{\delta}(y)$ versus y.

Block copolymer lamellae during directed assembly closely follow chemical surface patterns with supplemental roughness or, as shown previously, even more complex geometries.[23,37] The favorable interactions between the substrate pattern and the block copolymer domains overcome the free-energy penalty for deforming the lamellae away from their equilibrium structure.[37,43,44] Figure 4 shows SEM micrographs of the PS-*b*-PMMA lamellar morphology at the substrate surface (the bottom of the 40 nm thick block copolymer films, z = 0) when assembled on chemical surface patterns with L_{LER} = 140 and 70 nm undulation roughness. The interfaces between lamellar domains show clear undulation roughness at the substrate that indicates the supplemental roughness in the chemical surface pattern was imposed in the block copolymer interfaces near the substrate. The comparison of the block copolymer lamellae at the bottom of the film to those at the top of the film (Figure 2, parts b and c) further suggests that undulation roughness with L_{LER} = 70 nm was diminished more rapidly than roughness with L_{LER} = 140 nm. Defects observed in the lamellae of Figure 4 arose from defects in the corresponding chemical surface patterns. The process used to flip over the block copolymer films made it difficult to locate regions with perfect chemical surface patterns and long-range ordered block copolymers.

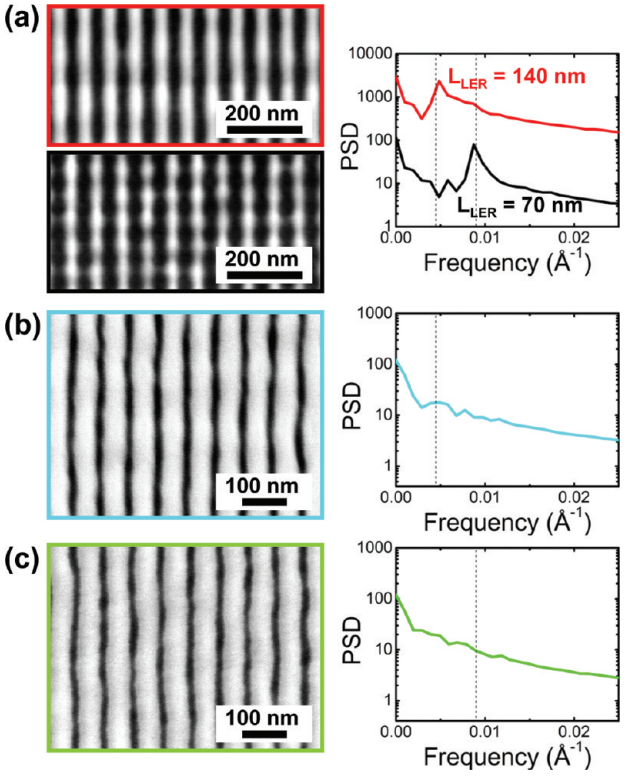

Figure 5. Characterization of PS-*b*-PMMA lamellae directed to assemble on chemical surface patterns with peristaltic roughness. (a) Top-down SEM images and PSD analyses of the line edge roughness for photoresist patterned with peristaltic roughness having L_{LER} = 140 nm (red, top frame) and 70 nm (black, bottom frame). (b) SEM image and PSD of block copolymer lamellae assembled on surface patterns with L_{LER} = 140 nm peristaltic roughness. (c) SEM image and PSD of block copolymer lamellae assembled on surface patterns with L_{LER} = 70 nm peristaltic roughness. The dashed vertical lines in the PSD plots indicate the frequencies corresponding to L_{LER} = 140 and 70 nm.

Peristaltic roughness in the chemical surface patterns decays rapidly in the interfaces of the assembled block copolymer lamellae. Chemical surface patterns with peristaltic roughness are characterized in Figure 5a and have clear peaks in the PSD analysis at the frequencies consistent with L_{LER} = 140 and 70 nm. The PS-*b*-PMMA lamellae on surface patterns with L_{LER} = 140 peristaltic roughness display a weak peak in the PSD curve, while lamellae on surface patterns with L_{LER} = 70 peristaltic roughness do not display enhanced line edge roughness at the expected frequency. The strength of the PSD peak for the L_{LER} = 140 case indicates that this roughness is not strongly correlated. A visual examination of the top-down SEM micrograph in Figure 5b suggests that the interfaces have noticeable roughness and there may exist a combination of out-of-phase and in-phase roughness. The spatially averaged interfaces, however, have a clear sinusoidal shape as shown in Figure 6 and provide a quantitative characterization of roughness in the peristaltic interfaces. The relative amplitudes of the average interface deformation were $f(z = 40 \text{ nm})/\delta_o$ = 0.30 and 0.066 for L_{LER} = 140 and 70 nm, respectively. Peristaltic roughness in the chemical surface patterns, much like undulation roughness, is diminished to varying extents depending on the roughness periodicity, with the L_{LER} = 140 nm roughness propagating through the lamellar domain interfaces more readily than the L_{LER} = 70 nm roughness.

Peristaltic structures are particularly unfavorable in block copolymer lamellae because they require large line width variations where the domains are significantly compressed and stretched. These unfavorable configurations of the polymer

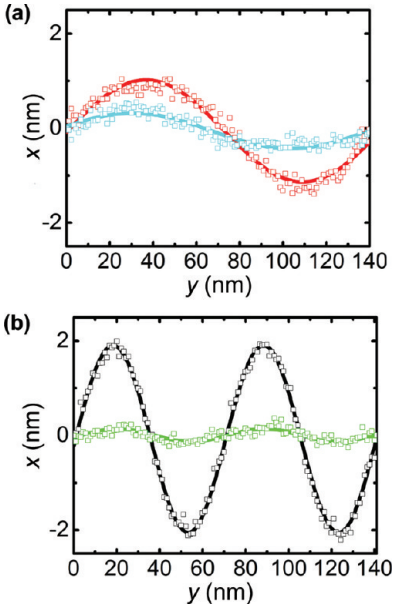

Figure 6. Average deformation $\bar{\delta}(y)$ of the experimental block copolymer interfaces and chemical surface patterns as a function of position along the interfaces (in the *y*-direction) for peristaltic surface pattern roughness with (a) L_{LER} = 140 nm and (b) L_{LER} = 70 nm. The experimental data and sinusoidal fits are shown as open circles and continuous curves of the same color, respectively. Red and black colors indicate the average shape of the chemical surface pattern, while blue and green colors indicate the lamellar interfaces at the top of the block copolymer film directed to assemble on such surfaces. The lamellar interfaces are assumed to be in-phase with the corresponding chemical surface pattern.

chains lead to higher free energies such that the block copolymer favors self-correcting for these line width variations by returning to the equilibrium lamellar morphology, in which the domain spacing is controlled by the polymer molecular weight and interfacial tension between domains. Consequently peristaltic roughness did not propagate from the surface pattern into the interface between block copolymer domains as readily as the undulation surface pattern roughness that had a relatively more uniform line width.

Molecular-level SCMF simulations were used to investigate the directed assembly of block copolymer lamellae on chemical surface patterns with roughness and to provide additional information regarding the propagation of the roughness throughout the thickness of the film. The oscillatory patterns of the experimental setup were modeled by patterns with an idealized line edge roughness and sinusoidal geometry (L_{LER} = 70 or 140 nm and amplitude δ_o = 6.16 nm), as shown in Figure 7, parts a (undulation pattern LER) and b (peristaltic pattern LER). The corresponding images of the free surface of the assembled block copolymer morphologies are shown in the same figure enclosed with light green or blue borders, with cutaways at z = 17.12 nm (lower right quarter of each snapshot) illustrating the deformation of the interfaces deeper in the film. Two descriptors of the average interface shape, identical to those provided in the experimental analysis, are used to quantify the effect of the surface pattern LER on the domain interfaces. First, the average shape of the interfaces on the free film surface is quantified via the PSD function which is shown in the lower row of Figure 7, for undulation (left) and peristaltic (right) surface pattern LER. The simulations describe the three-dimensional structure of the assembled morphologies,[32] therefore, unlike the experiments, the average deformation of the interface shape can be easily obtained as a function of the distance from the patterned substrate throughout the entire film. Second, Figure 8 shows the simulation

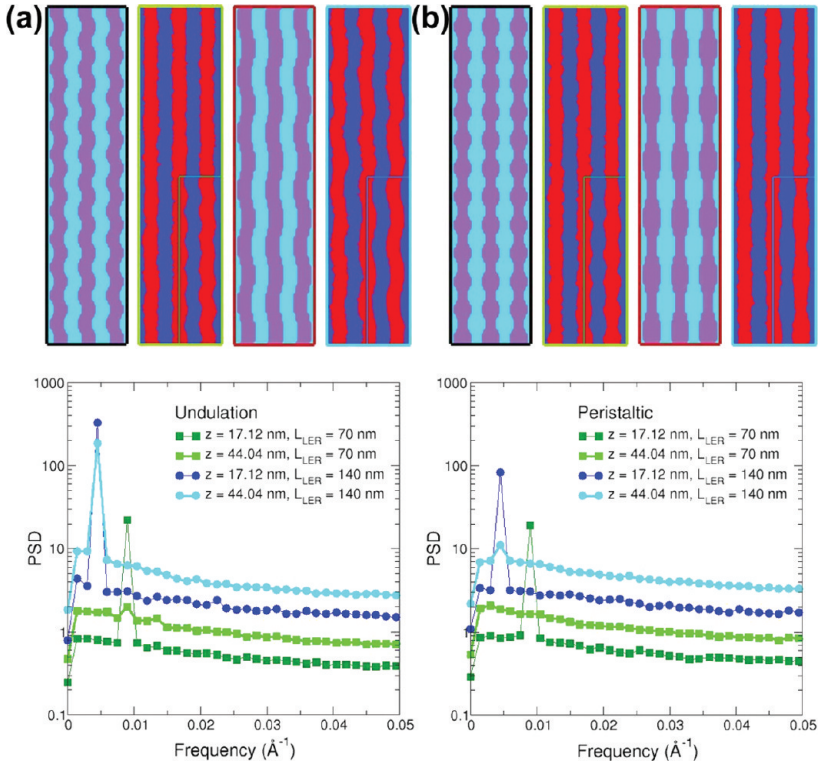

Figure 7. Single-Chain-in-Mean-Field simulation results of block copolymer films assembled on chemical surface patterns with (a) undulation and (b) peristaltic roughness. Top row: Top-down images of the chemically patterned surfaces (enclosed with black or red borders for L_{LER} = 70 and 140 nm, respectively) and the PS-*b*-PMMA lamellae assembled on such surfaces (enclosed with light green or light blue borders for L_{LER} = 70 and 140 nm, respectively) are shown as snapshots from the SCMF simulations. The PS-rich and the PMMA-rich domains in the block copolymer structures are illustrated in red and blue, respectively. The main area of each snapshot of the block copolymer structure demonstrates the top surface of the film (at z = 44.04 nm), while the cutaway, on the bottom-right of each snapshot and enclosed in a dark green or dark blue box, shows the morphology deeper in the film at a distance of z = 17.12 nm from the substrate. Bottom row: SCMF simulation results for the power spectra density of the PS/PMMA interface calculated at distances from the substrate of z = 17.12 nm (dark colors) and 44.04 nm, *i.e.*, the top surface of the film (light colors). Results are reported for surface patterns with roughness having periodicities of L_{LER} = 70 nm (green squares) and 140 nm (blue circles).

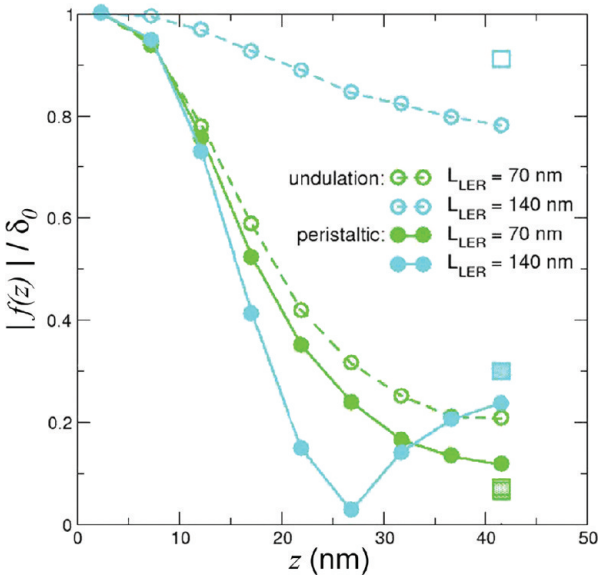

Figure 8. Comparison of the relative amplitude of the lamellar interface deformation $|f(z)|/\ \delta_o$ between the experimental results at the top surface of the film (boxes) and the predictions of the Single-Chain-in-Mean-Field simulations throughout the film (circles and solid lines). The simulated L_{LER}, L_O, and H match the experimentally examined cases.

predictions for the average deformation of the block copolymer interface by plotting $|f(z)|/\ \delta_o$ as a function of the distance from the chemical surface pattern, z. The $f(z)$ was determined, as discussed previously for the experiments, by fitting the time-averaged interface position $\bar{\delta}(y,z)$ to a simple, trigonometric expression with the appropriate periodicity ($h(y,z) = f(z)$ sin$(2\pi y/L_{LER})$). Figure 8 also includes data points for $|f(z)|/\ \delta_o$ from the experimental results of the average block copolymer interface at the top surface of the film, as analyzed in Figures 3 and 6, for comparison with the simulation predictions.

The predictions from the SCMF simulations regarding the average interface deformation qualitatively match the experimental observations for PS-*b*-PMMA lamellae shown in Figures 2−6. The small relative deformation amplitude, $|f(z)|/\ \delta_o$, demonstrates that both the undulation and peristaltic surface pattern roughness with L_{LER} = 70 nm does not propagate in the block copolymer interfaces through the entire film. The corresponding PSDs (light green curves) are in full agreement with the experiments and the $|f(z)|/\ \delta_o$ data, and illustrate that L_{LER} = 70 nm surface pattern roughness is almost fully remedied in the block copolymer structures at the top of the film. Weak PSD signals could still be observed in the SCMF simulations addressing systems with an idealized line edge roughness in the surface pattern, but were not recorded in the corresponding experimental systems (see Figures 2c and 5c). The CD−SEM characterization technique or deviations in the underlying surface pattern from an ideal sinusoidal geometry possibly obscured the observation of such peaks in the PSDs of the experimental systems. In contrast, the PSD curves calculated deeper in the film at z = 17.12 nm (dark green curves) show a clear peak at the characteristic roughness frequency for both geometries of L_{LER} = 70 nm

roughness and demonstrates the strong interface deformation near the patterned substrate.

The strong propagation of the L_{LER} = 140 nm undulation roughness through the 40 nm thick film is confirmed by the well-defined peak in the PSD curve and is consistent with the experimental results. Only an approximate 20% decay of the deformation amplitude $|f(z)|/\delta_o$ is observed on the free surface (see Figure 8) and is similar to the 9% decay measured in the experiments. For the L_{LER} = 140 nm peristaltic roughness in the surface pattern, the SCMF simulations predict a significant reduction of the interface deformation on the top of the film (note the weak peak in the corresponding PSD, light blue curve). The magnitudes of the average interface deformation show excellent quantitative agreement between the experiments and simulations for all types of examined roughness in the surface pattern, including the L_{LER} = 140 nm peristaltic roughness case (~75% and ~70% decay in $|f(z)|/\delta_o$ for the simulations and experiments, respectively). A 180° phase change in the average deformation of the lamellar interface with respect to the underlying pattern is also predicted in the simulations, as indicated by the nonmonotonic behavior of the solid, light blue curve (see ref 32 for additional details regarding this phase inversion phenomenon). Although the phase of the lamellar interfaces relative to the surface pattern has not been determined in the experiments, the consistency between the amplitudes of deformation suggests that phase inversion in the L_{LER} = 140 nm peristaltic roughness case may be occurring in the experimental systems. Overall the SCMF simulations predict that the peristaltic surface pattern roughness is dampened more quickly than the analogous undulation surface pattern roughness.

Conclusions

Directed assembly of block copolymers with chemically patterned substrates is an effective strategy for fabricating microelectronics oriented nanostructures. State-of-the-art fabrication techniques can create chemical surface patterns with the desired geometries and layouts, but small deviations of the edges from the ideal shapes are possible due to the complex chemical patterning process. In this work the ability of copolymer materials to rectify the line edge roughness in chemical patterns used to guide the self-assembly process was demonstrated experimentally, thereby confirming predictions obtained from a phenomenological theory and molecular-level simulations.[32] The propagation of roughness in the domain interfaces of lamellar copolymer structures was considered by purposefully creating chemically striped surfaces with controlled LER. Descriptors quantifying the average shape of the block copolymer interfaces were used to determine the interface roughness on the free surface and, in the molecular-level simulations, throughout the film. The propagation of interface roughness in the block copolymer structures, as induced by the surface pattern roughness, was shown to depend upon its characteristic wavelength, geometry, and distance from the substrate. In particular, larger wavelength LER in the surface pattern was demonstrated to affect the copolymer interfaces farther into the film from the substrate. Both the experimental and simulation results show that the interface deformation generated by surface pattern roughness with peristaltic geometries diminished more rapidly than undulation geometries with distance from the substrate. This observation can be explained by the large distortions of the lamellar spacing and polymer chain configurations induced by the peristaltic geometries.

The ability of block copolymers to reduce LER may be enhanced through careful design of the copolymer components, possibly by choosing systems with a greater degree of incompatibility leading to stronger segregation. Further characterization of the line edge roughness and self-healing properties of block copolymers also must consider rough surface patterns with a broad spectrum of LER wavelengths, as well as the impact of the intrinsic width of the interfaces and capillary waves induced by thermal fluctuations on the self-assembled structures. As a final note, the application of these materials and techniques for advanced lithography will require selective removal of one block of the assembled structures to create a soft mask for subsequent pattern transfer processes.[15,45,46] Future studies should examine the influence of these additional processing steps on the LER of the block copolymer structures and the patterns transferred to the substrate.[47,48]

Acknowledgment. Support was provided by the Semiconductor Research Corporation (No. 2005−OCH-985), the NSF UW Nanoscale Science and Engineering Center (No. DMR-0425880), and the Volkswagen Foundation. This work made use of the facilities and staff at the UW Synchrotron Radiation Center (NSF Grant No. DMR-0084402), the UW Center for Nanotechnology, and the John von Neumann-Institute for Computing, Jülich, Germany. MPS thanks the Graduate Fellowship Program of the Semiconductor Research Corporation for financial support and Chi-Chun Liu for useful discussions.

References and Notes

(1) Semiconductor Industry Association, International Technology Roadmap for Semiconductors , **2007**.
(2) Padmanaban, M.; Rentkiewicz, D.; Hong, C.; Lee, D.; Rahman, D.; Sakamuri, R.; Dammel, R. R. *J. Photopolym. Sci. Technol.* **2005**, *18*, 451–456.
(3) Constantoudis, V.; Patsis, G. P.; Tserepi, A.; Gogolides, E. *J. Vac. Sci. Technol., B* **2003**, *21*, 1019–1026.
(4) Yamaguchi, A.; Fukuda, H.; Arai, T.; Yamamoto, J.; Hirayama, T.; Shiono, D.; Hada, H.; Onodera, J. *J. Vac. Sci. Technol., B* **2005**, *23*, 2711–2715.
(5) Yamaguchi, A.; Komuro, O. *Jpn. J. Appl. Phys., Part 1* **2003**, *42*, 3763–3770.
(6) Lorusso, G. F.; Leunissen, P.; Ercken, M.; Delvaux, C.; Van Roey, F.; Vandenbroeck, N.; Yang, H.; Azordegan, A.; DiBlase, T. *J. Microlith. Microfab. Microsys.* **2006**, *5*, 033003.
(7) Steinhögl, W.; Schindler, G.; Steinlesberger, G.; Traving, M.; Engelhardt, M. *Microelectron. Eng.* **2004**, *76*, 126–130.
(8) Stucchi, M.; Bamal, M.; Maex, K. *Microelectron. Eng.* **2007**, *84*, 2733–2737.
(9) Asenov, A.; Kaya, S.; Brown, A. R. *IEEE Trans. Electron Devices* **2003**, *50*, 1254–1260.
(10) Kim, H.-W.; Lee, J.-Y.; Shin, J.; Woo, S.-G.; Cho, H.-K.; Moon, J.-T. *IEEE Trans. Electron Devices* **2004**, *51*, 1984–1988.
(11) Hawker, C. J.; Russell, T. P. *MRS Bull.* **2005**, *30*, 952–966.
(12) Segalman, R. A. *Mater. Sci. Eng., Res.* **2005**, *48*, 191–226.
(13) Stoykovich, M. P.; Nealey, P. F. *Mater. Today* **2006**, *9*, 20–29.
(14) Ross, C. A.; Cheng, J. Y. *MRS Bull.* **2008**, *33*, 838–845.
(15) Park, M.; Harrison, C.; Chaikin, P. M.; Register, R. A.; Adamson, D. H. *Science* **1997**, *276*, 1401–1404.
(16) Bates, F. S.; Fredrickson, G. H. *Annu. Rev. Phys. Chem.* **1990**, *41*, 525–557.
(17) Bates, F. S.; Fredrickson, G. H. *Phys. Today* **1999**, *52*, 32–38.
(18) Rockford, L.; Liu, Y.; Mansky, P.; Russell, T. P.; Yoon, M.; Mochrie, S. G. J. *Phys. Rev. Lett.* **1999**, *82*, 2602–2605.
(19) Yang, X. M.; Peters, R. D.; Nealey, P. F.; Solak, H. H.; Cerrina, F. *Macromolecules* **2000**, *33*, 9575–9582.
(20) Rockford, L.; Mochrie, S. G. J.; Russell, T. P. *Macromolecules* **2001**, *34*, 1487–1492.
(21) Kim, S. O.; Solak, H. H.; Stoykovich, M. P.; Ferrier, N. J.; de Pablo, J. J.; Nealey, P. F. *Nature* **2003**, *424*, 411–414.
(22) Stoykovich, M. P.; Muller, M.; Kim, S. O.; Solak, H. H.; Edwards, E. W.; de Pablo, J. J.; Nealey, P. F. *Science* **2005**, *308*, 1442–1446.
(23) Stoykovich, M. P.; Kang, H.; Daoulas, K. C.; Liu, G.; Liu, C. C.; de Pablo, J. J.; Mueller, M.; Nealey, P. F. *ACS Nano* **2007**, *1*, 168–175.
(24) Cheng, J. Y.; Rettner, C. T.; Sanders, D. P.; Kim, H. C.; Hinsberg, W. D. *Adv. Mater.* **2008**, *20*, 3155–3158.
(25) Bita, I.; Yang, J. K. W.; Jung, Y. S.; Ross, C. A.; Thomas, E. L.; Berggren, K. K. *Science* **2008**, *321*, 939–943.

(26) Ruiz, R.; Kang, H. M.; Detcheverry, F. A.; Dobisz, E.; Kercher, D. S.; Albrecht, T. R.; de Pablo, J. J.; Nealey, P. F. *Science* **2008**, *321*, 936–939.
(27) Petera, D.; Muthukumar, M. *J. Chem. Phys.* **1998**, *109*, 5101–5107.
(28) Chen, H.; Chakrabarti, A. *J. Chem. Phys.* **1998**, *108*, 6897–6905.
(29) Pereira, G. G.; Williams, D. R. M. *Macromolecules* **1999**, *32*, 758–764.
(30) Tsori, Y.; Andelman, D. *Europhys. Lett.* **2001**, *53*, 722–728.
(31) Wu, X. F.; Dzenis, Y. A. *J. Chem. Phys.* **2006**, *125*, 174707.
(32) Daoulas, K. C.; Muller, M.; Stoykovich, M. P.; Kang, H.; de Pablo, J. J.; Nealey, P. F. *Langmuir* **2008**, *24*, 1284–1295.
(33) Edwards, E. W.; Muller, M.; Stoykovich, M. P.; Solak, H. H.; de Pablo, J. J.; Nealey, P. F. *Macromolecules* **2007**, *40*, 90–96.
(34) Edwards, E. W.; Montague, M. F.; Solak, H. H.; Hawker, C. J.; Nealey, P. F. *Adv. Mater.* **2004**, *16*, 1315–1319.
(35) Stoykovich, M. P.; Edwards, E. W.; Solak, H. H.; Nealey, P. F. *Phys. Rev. Lett.* **2006**, *97*, 147802.
(36) Daoulas, K. C.; Müller, M.; de Pablo, J. J.; Nealey, P. F.; Smith, G. D. *Soft Matter* **2006**, *2*, 573–583.
(37) Daoulas, K. C.; Muller, M.; Stoykovich, M. P.; Park, S. M.; Papakonstantopoulos, Y. J.; de Pablo, J. J.; Nealey, P. F.; Solak, H. H. *Phys. Rev. Lett.* **2006**, *96*, 036104.
(38) Muller, M.; Smith, G. D. *J. Polym. Sci., Part B: Polym. Phys.* **2005**, *43*, 934–958.
(39) Daoulas, K. C.; Müller, M. *J. Chem. Phys.* **2006**, *125*, 184904.
(40) Daoulas, K. C.; Müller, M. *Adv. Polym. Sci.* **2010**, *224*, 197–233.
(41) Müller, M.; Schmid, F. *Adv. Polym. Sci.* **2005**, *185*, 1–58.
(42) Helfand, E.; Tagami, Y. *J. Chem. Phys.* **1972**, *56*, 3592–3601.
(43) Knoll, A.; Horvat, A.; Lyakhova, K. S.; Krausch, G.; Sevink, G. J. A.; Zvelindovsky, A. V.; Magerle, R. *Phys. Rev. Lett.* **2002**, *89*, 035501.
(44) Rehse, N.; Knoll, A.; Magerle, R.; Krausch, G. *Macromolecules* **2003**, *36*, 3261–3271.
(45) Thurn-Albrecht, T.; Steiner, R.; DeRouchey, J.; Stafford, C. M.; Huang, E.; Bal, M.; Tuominen, M.; Hawker, C. J.; Russell, T. P. *Adv. Mater.* **1997**, *12*, 787–791.
(46) Liu, C. C.; Nealey, P. F.; Ting, Y. H.; Wendt, A. E. *J. Vac. Sci. Technol., B* **2007**, *25*, 1963–1968.
(47) Goldfarb, D. L.; Mahorowala, A. P.; Gallatin, G. M. P., K. E.; Rasgon, S.; Sawin, H. H.; Allen, S. D.; Lawson, M. C.; Kwong, R. W. *J. Vac. Sci. Technol., B* **2004**, *22*, 647–653.
(48) Pawloski, A. R.; Acheta, A.; Bell, S.; La Fontaine, B.; Wallow, T.; Levinson, H. J. *Proc. SPIE, Adv. Resist Technol. Process. XXIII* **2006**, *6153*, 615318.